

Momentum Contrastive Voxel-wise Representation Learning for Semi-supervised Volumetric Medical Image Segmentation

Chenyu You¹, Ruihan Zhao², Lawrence Staib¹, James S. Duncan¹

¹Yale University

²University of California, Berkeley

Abstract. Automated segmentation in medical image analysis is a challenging task that requires a large amount of manually labeled data. However, manually annotating medical data is often laborious, and most existing learning-based approaches fail to accurately delineate object boundaries without effective geometric constraints. Contrastive learning, a sub-area of self-supervised learning, has recently been noted as a promising direction in multiple application fields. In this work, we present a novel **C**ontrastive **V**oxel-wise **R**epresentation **D**istillation (CVRD) method with geometric constraints to learn global-local visual representations for volumetric medical image segmentation with limited annotations. Our framework can effectively learn global and local features by capturing 3D spatial context and rich anatomical information. Specifically, we introduce a voxel-to-volume contrastive algorithm to learn global information from 3D images, and propose to perform local voxel-to-voxel distillation to explicitly make use of local cues in the embedding space. Moreover, we integrate an elastic interaction-based active contour model as a geometric regularization term to enable fast and reliable object delineations in an end-to-end learning manner. Results on the Atrial Segmentation Challenge dataset demonstrate superiority of our proposed scheme, especially in a setting with a very limited number of annotated data. The code will be available at <https://github.com/charlesyou999648/CVRD>.

1 Introduction

Learning from just a few labeled examples while leveraging a large amount of unlabeled data is the long-standing pursuit in the machine learning community, which is especially crucial for the medical imaging domain. Generating reliable manual annotations of 3D imaging data at scale is expensive, time-consuming, and may require domain-specific expertise. Due to privacy concerns, another challenge in medical imaging is relatively small training datasets. To this end, contrastive learning based self-supervised learning (SSL) has drawn considerable attention to learn useful representations without human supervision and shown remarkable performance in vision tasks [1, 3, 6, 19]. In addition, convolutional neural networks (CNNs) have given rise to human-level performance in several computer vision tasks, *e.g.*, semantic segmentation. As noted in [17, 55],

CNNs often perform poorly on accurate delineations of object boundaries. Consequently, it is necessary to incorporate robust geometric constraints to improve topological accuracy.

Our work draws on existing related literature in self-supervised learning, semi-supervised learning, and geometric priors. SSL [13, 33, 58] aims to learn effective visual representations from unlabeled data in an unsupervised setting. In recent years, a growing popularity of work [3, 5, 6, 15, 25, 26, 28, 31, 37, 39, 43–45, 47, 47, 53] in contrastive learning has brought significant progress in SSL. The central idea is to learn powerful representations that optimize similarity constraints to discriminate similar (positive) and dissimilar (negative) pairs within a dataset. The major stream of subsequent work focuses on the choice of dissimilar pairs which decide the quality of learned representations. The loss function used to contrast is chosen from several options, such as InfoNCE [34], Triplet [38], and so on. Recently, Chaitanya *et al.* [3] extended contrastive learning framework to learn global and local cues, which require large amounts of negative pairs. Second, the recent analysis [6] has suggested that large batch size may achieve stronger performance gains, but such training is expensive in terms of both time and computational resource. Third, most works mainly focus on exploring 2D/2.5D context instead of 3D space.

In the medical imaging domain, substantial efforts [2, 4, 9–12, 14, 21, 22, 24, 27, 32, 40, 42, 46–52, 54, 56] have been devoted to incorporating unlabeled data to improve network performance due to the limited 3D data and annotations. The most commonly training techniques are adversarial learning and consistency loss as regularization terms to encourage unsupervised mapping. Nie *et al.* [32] adopted adversarial training to select confident regions of unlabeled images for segmentation performance improvements. Yu *et al.* [54] designed a deep uncertainty-aware framework based on the mean-teacher scheme [36] to guide the student network to capture better features. Despite having success in superior performance gains, these methods ignore the intrinsic geometric structure of the image, such as border, which may fail in recognizing object contours. Li *et al.* [23] proposed to utilize signed distance fields for boundary prediction to achieve superior segmentation performance improvements.

In order to address the aforementioned challenges, several efforts [18, 23, 41, 57] have attempted to leverage shape priors to detect more accurate boundaries. Although those methods have achieved promising results, they may not guarantee a target topology in the test stage. Active Contour Models (ACM) [20] is a set of algorithms that, given an initial contour, dynamically fit an image boundary with geometric constraints. Thus, it may be appropriate in such cases, especially in medical imaging where the training dataset is too small to train a deep segmentation network. Recent works [7, 8, 17, 29, 55] used the energy function as the part of supervised loss in an end-to-end manner. However, these methods lack learning efficiency and suffer from a time-consuming mechanism that only involves comparing two binary images at a time.

In this paper, we present CVRD, an end-to-end semi-supervised framework that integrates contrastive distillation with geometric constraints to learn global

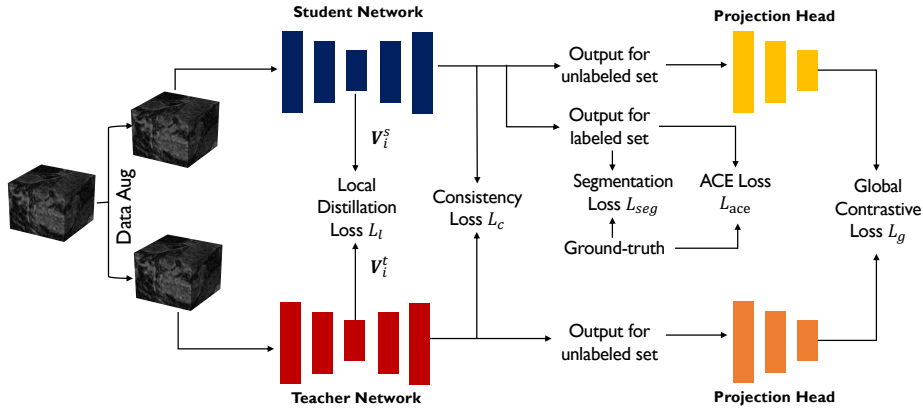


Fig. 1: Overview of CVRD architecture. We learn rich dense voxel-wise representations by exploiting global context between voxels and volumetric regions and local correlations among voxels for semi-supervised segmentation.

contexts and local features for more effective representation learning in 3D imaging. The motivation comes from the fact that feature presentations derived on the 2D context fail to utilize useful spacial contexts in the 3D domain, which may result in a huge performance degradation. Two key aspects distinguish from the recent advance [3]. First, in contrast to follow the standard contrastive learning setting [6] to perform slice-level global contrast, we perform voxel-to-volume global contrast in 3D embedding space, which could capture rich anatomic information. Second, we propose an additional voxel-to-voxel local distillation to exploit distinctive features in the latent feature space. The third important aspect concerns time and computational costs, which is challenging to apply in most real-wold applications.

Our contributions are three-fold: (1) we propose two learning strategies - global voxel-to-volume contrast and local voxel-to-voxel distillation - to better utilize unlabeled data, which capture higher-order consistency in the well-structured global embedding space while making full use of voxel-wise similarities of the local context; (2) To address occasional inaccuracies along object boundaries, we then incorporate an active contour with elastica (ACE) loss as the regularization term for penalization on curvature region and accurate edge placements; (3) The results demonstrate that our segmentation network outperforms the state-of-the-art methods on the Atrial Segmentation Challenge dataset, and generates object segmentation with high-quality global shapes.

2 Method

2.1 Overview

We aim at constructing an end-to-end voxel-wise representation learning algorithm with geometric constraints to learn useful representations in discriminative manner for semi-supervised volumetric medical imaging segmentation. An

overview of the architecture is illustrated in Figure 1. In the limited annotation setting, we train semi-supervised CVRD alongside two components - supervised and unsupervised learning objectives. Specifically, we propose a novel voxel-wise representation learning algorithm to learn global-level and local-level representations from 3D unlabeled data by regularizing the embedding space and exploring the geometric and spatial context of training voxels. The ACM model further enables the segmentation network to capture more rich details of image boundaries.

In our problem setting, we consider a set of training data (3D images) including N labeled data and M unlabeled data, where $N \ll M$. For simplicity of exposition, we denote limited label data as $\mathcal{D}_l = \{(\mathbf{x}_i, y_i)\}_{i=1}^N$, and abundant unlabeled data as $\mathcal{D}_u = \{(\mathbf{x}_i)\}_{i=N+1}^{N+M}$, where $\mathbf{x}_i \in \mathbb{R}^{H \times W \times D}$ are volume inputs, and $y_i \in \{0, 1\}^{H \times W \times D}$ are ground-truth labels. Specifically, we adopt V-Net [54] as the network backbone $F(\cdot)$, which consists of an encoder network $e(\cdot)$ and a decoder network $d(\cdot)$. To maximize mutual information between latent representations, we design a projection head $G(\cdot)$, that comprises one encoder network which is similar to $e(\cdot)$, and followed by 3-layer multilayer perceptron (MLP).

2.2 Unsupervised Contrastive Distillation

A key component of CVRD is the ability to capture rich voxel-wise representations of high dimensional data by contrastive distillation. CVRD trains the contrastive objective as an auxiliary loss during the volume batch updates. To specify our voxel-wise contrastive algorithm, we define two discrimination terms: (i) global contrastive objective (ii) local distillation objective. Specification of these aspects largely influence quality of learned representations.

Global Contrastive Loss \mathcal{L}_g CVRD performs global voxel-to-volume contrast by using a novel 3D projection head $G(\cdot)$. Different from the standard setting [3, 6] of using MLP, which are designed for 2D image-level data, $G(\cdot)$ can encode rich spatial information, which can build a stronger ability to model spatial correlations in high-dimensional 3D space. To learn embeddings that measure these similarity relations across volumes, here we use InfoNCE loss [34]:

$$\mathcal{L}(\mathbf{u}, \mathbf{u}^+) = -\log \frac{\exp(\mathbf{u} \cdot \mathbf{u}^+ / \tau_g)}{\exp(\mathbf{u} \cdot \mathbf{u}^+ / \tau_g) + \sum_{\mathbf{u}^- \in \mathcal{N}_t^-} \exp(\mathbf{u} \cdot \mathbf{u}^- / \tau_g)}, \quad (1)$$

where \mathbf{u} is the embedding of transformed version of the same \mathbf{x} , *i.e.* $\mathbf{u} = G(F(t(\mathbf{x})))$ where $t \in \mathcal{T}$ are simple random 3D transformations (*e.g.*, random flipping, random rotation, random brightness, random contrast, random zooming, cube rearrangement and cube rotation). Similarly, \mathbf{u}^+ , and \mathbf{u}^- are referred to as positive, and negative respectively in the parlance of contrastive learning. Here we denote ‘ \cdot ’ as the inner (dot) product [39], and $\tau_g > 0$ denotes a temperature parameter for \mathcal{L}_g . Recent work [39] shows that a large set of negatives (*i.e.*, $|\mathcal{N}_t^-|$) can improve the quality of learned representations in unsupervised contrastive training. In our experiments, we include all other feature maps

except only the feature map itself from the same volume batches as negatives. In the unlabeled set, our global contrastive loss is defined as:

$$\mathcal{L}_g = \frac{1}{|\mathcal{N}_I^+|} \sum_{\forall(\mathbf{u}, \mathbf{u}^+) \in \mathcal{N}_I^+} [\mathcal{L}(\mathbf{u}, \mathbf{u}^+) + \mathcal{L}(\mathbf{u}^+, \mathbf{u})], \quad (2)$$

where \mathcal{N}_I^+ denotes embedding collections of the positive volume samples.

Local Distillation Loss \mathcal{L}_l The motivation of local distillation objectives is designed to extract discriminative local representations, which serve as a bridge to correlate the voxel-wise representations of the output feature domain and the latent feature domain. Therefore, we propose to perform voxel-to-voxel local distillation to explicitly explore local relationships between voxel samples. In implementations, we utilize the encoders e_t and e_s to extract the distinct local features \mathbf{V} , acquiring the student hidden embeddings $\mathbf{V}_i^s \in \mathbb{R}^{H'W'D' \times D_e}$ and the teacher hidden embeddings $\mathbf{V}_i^t \in \mathbb{R}^{H'W'D' \times D_e}$, respectively. Thus, our local distillation loss can be formulated as:

$$\mathcal{L}_l = -\frac{1}{M} \sum_{i=N+1}^{N+M} \sum_{j=1}^{H'W'D'} \log \frac{\exp(\cos(\mathbf{v}_{i,j}^s, \mathbf{v}_{i,j}^t))}{\sum_k \exp(\cos(\mathbf{v}_{i,j}^s, \mathbf{v}_{i,k}^t))}, \quad (3)$$

where $\mathbf{v}_{i,j}$ be the j th row of \mathbf{V}_i , and $\cos(\mathbf{v}_1, \mathbf{v}_2) = \frac{\mathbf{v}_1 \cdot \mathbf{v}_2}{\|\mathbf{v}_1\| \|\mathbf{v}_2\|}$ denotes the cosine similarity loss.

2.3 Semi-supervised CVRD Implementation

CVRD is a general semi-supervised framework for combining contrastive distillation with geometric constraints. In our experiments, we train CVRD alongside two strategy - supervised objective and unsupervised objective.

Consistency Loss \mathcal{L}_c Recent work [21, 36] show that using an exponential moving average (EMA) over network parameters is empirically shown to improve training stability and models' final performance. With this insight, we introduce an EMA model with parameters θ as the moving-average of the parameters θ' from the original network. Specifically, the architecture of EMA model follows the original model. At training step t , the update rule follows $\theta_t = m\theta_{t-1} + (1 - m)\theta'_t$, where $m \in [0, 1]$ is momentum parameter. On the unlabeled set, we perform different perturbation operations on the unlabeled input volume sample \mathbf{x}^u , *e.g.* adding noise ϵ . To encourage training stability and performance improvements, we define consistency loss as:

$$\mathcal{L}_c = \mathcal{L}_{\text{mse}}(F(\mathbf{x}^u; \theta, \epsilon), F(\mathbf{x}^u; \theta', \epsilon')), \quad (4)$$

where \mathcal{L}_{mse} is the mean squared error loss.

Table 1: Quantitative segmentation results on the LA dataset. The backbone network of all evaluated methods are V-Net.

Method	# scans used		Metrics			
	Labeled	Unlabeled	Dice[%]	Jaccard[%]	ASD[voxel]	95HD[voxel]
V-Net [30]	80	0	91.14	83.82	1.52	5.75
V-Net	16	0	86.03	76.06	3.51	14.26
DAP [57]	16	64	87.89	78.72	2.74	9.29
UA-MT [54]	16	64	88.88	80.21	2.26	7.32
LG-ER-MT [16]	16	64	89.56	81.22	2.06	7.29
SASSNet [23]	16	64	89.27	80.82	3.13	8.83
Chaitanya <i>et al.</i> [3]	16	64	89.94	81.82	2.66	7.23
CVRD(ours)	16	64	90.34	82.92	1.87	6.72
V-Net [30]	8	0	79.99	68.12	5.48	21.11
DAP [57]	8	72	81.89	71.23	3.80	15.81
UA-MT [54]	8	72	84.25	73.48	3.36	13.84
LG-ER-MT [16]	8	72	85.43	74.95	3.75	15.01
SASSNet [23]	8	72	86.81	76.92	3.94	12.54
Chaitanya <i>et al.</i> [3]	8	72	84.95	74.77	3.70	10.68
CVRD(ours)	8	72	88.53	78.80	2.91	9.20

Overall Training Objective Our overall learning objective is to minimize a combination of supervised and unsupervised losses. On the labeled data, we incorporate ACE loss [7] as geometric constraints in training. On the unlabeled dataset, unsupervised training objective consist of global contrastive loss, local distillation loss, and consistency loss. The overall loss function is:

$$\mathcal{L} = \underbrace{\mathcal{L}_{seg} + \lambda \mathcal{L}_{ace}}_{\text{supervised}} + \underbrace{\alpha \mathcal{L}_g + \beta \mathcal{L}_l + \gamma \mathcal{L}_c}_{\text{unsupervised}}, \quad (5)$$

where $\lambda, \alpha, \beta, \gamma$ are hyperparameters that balance each term. \mathcal{L}_{seg} denotes the segmentation loss, and \mathcal{L}_{ace} is the ACE loss. More details about ACE loss can be found in [7].

3 Experiments

3.1 Dataset and Pre-processing

We conduct our experiments on the Left Atrium (LA) dataset from Atrial Segmentation Challenge¹. The dataset comprises of 100 3D gadolinium-enhanced MR imaging scans (GE-MRIs) with expert annotations, with an isotropic resolution of $0.625 \times 0.625 \times 0.625 \text{mm}^3$. Following the experimental setting in [54], we use 80 scans for training, and 20 scans for evaluation. We employ the same pre-processing methods by cropping all the scans at the heart region and normalized as zero and unit variance.

¹ <http://atriaseg2018.cardiacatlas.org/>

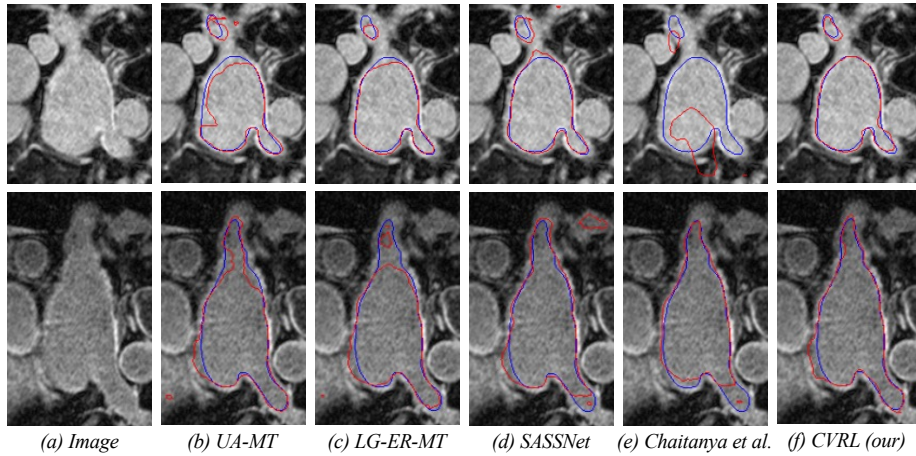


Fig. 2: Visual comparisons with other methods. As observed, our CVRD achieves superior performance with more accurate borders and shapes.

3.2 Implementation Details

In our framework, we use V-Net as the network backbone for two networks. All the training sub-volumes are augmented by random cropping to $112 \times 112 \times 80\text{mm}^3$. For data augmentation, we use standard data augmentation techniques [35, 54]. We empirically set the hyper-parameters $\lambda, \alpha, \beta, \gamma, \tau_g, \tau_l$ as 0.0001, 0.1, 0.1, 0.1, 0.1, 1.0, respectively. We use SGD optimizer with a momentum 0.9 and weight decay 0.0005 to optimize the network parameters. The initial learning rate is set as 0.01 and divided by 10 every 3000 iterations. For EMA updates, we follow the experimental setting in [54], where the EMA decay rate α is set to 0.999. We use the time-dependent Gaussian warming-up function $\Psi_{con}(t) = \exp(-5(1 - t/t_{max})^2)$ to ramp up parameters, where t and t_{max} denote the current and the maximum training step, respectively. For fairness, all evaluated methods are implemented in PyTorch, and trained for 6000 iterations on an NVIDIA 1080Ti GPU with batch size 4.

In the testing stage, we adopt four metrics to evaluate the segmentation performance, including Dice coefficient (Dice), Jaccard Index (Jaccard), 95% Hausdorff Distance (95HD), and Average Symmetric Surface Distance (ASD).

3.3 Comparison with Other Semi-supervised Methods

We evaluate our CVRD with several state-of-the-art semi-supervised segmentation methods on different amounts of labeled data, including V-Net [30], DAP [57], UA-MT [54], LG-ER-MT [16], SASSNet [23], and Chaitanya *et al.* [3]. Table 1 compares our segmentation results with other methods.

We first conduct experiments under 20% annotation ratios (16 labeled and 64 unlabeled). Under this setting, most above approaches achieve superior segmentation performance. CVRD gives slightly better performance thanks to its global

Table 2: Ablation study for the key component modules of CVRD on the LA dataset with 10% annotation ratio (8 labeled and 72 unlabeled).

Method	# scans used		Metrics			
	Labeled	Unlabeled	Dice[%]	Jaccard[%]	ASD[voxel]	95HD[voxel]
Baseline	8	72	83.09	71.75	5.53	19.65
Baseline+ \mathcal{L}_g	8	72	87.32	78.02	2.99	10.03
Baseline+ \mathcal{L}_l	8	72	87.11	77.03	3.74	12.31
Baseline+ \mathcal{L}_{ace}	8	72	85.77	75.39	5.17	18.98
Baseline+ $\mathcal{L}_g+\mathcal{L}_l$	8	72	87.93	78.01	2.97	9.63
Baseline+ $\mathcal{L}_g+\mathcal{L}_l+\mathcal{L}_{ace}$	8	72	88.53	78.80	2.91	9.20

and local voxel-wise feature extraction. In particular, our proposed method can be further improved with NMS, outperforming other end-to-end semi-supervised methods in Dice (90.34%), Jaccard (82.92%), ASD (1.87), and 95HD (6.72).

To further evaluate the effectiveness of CVRD, we compare it with other methods in 10% annotation ratio (8 labeled and 72 unlabeled), as reported in Table 1. We observe consistent performance improvements over state-of-the-arts, in terms of Dice (88.53%), and Jaccard (78.80%). Meanwhile, the results in Table 1 suggest that with NMS, CVRD achieves consistent performance gains. This evidence that i). taking voxel samples with contrastive learning yields better voxel embeddings; ii) both global voxel-to-volume and local voxel-to-voxel relations are informative cues; iii) utilizing an active contour model is capable of helping identify more accurate boundaries. Leveraging all these aspects, it can observe consistent performance gains. As shown in Fig. 2, our method is capable of generating more accurate segmentation, considering the fact the improvement in such setting is difficult. This demonstrates i) the necessity of comprehensively considering both global voxel-to-volume contrast and local voxel-to-voxel contrast; and ii) efficacy of elastica (curvature and length) and region constraints.

3.4 Ablation Study

We perform ablation experiments to validate the effectiveness of major components in our proposed method, including global contrastive strategy (global projection head), local distillation strategy, and ACE loss. The quantitative results is reported in Table 2. We compare CVRD with its five variants under 10% annotation ratio (8 labeled and 72 unlabeled). Specially, the Baseline model refers to UA-MT-UN [54] without uncertainty measures. We gradually incorporate \mathcal{L}_g , \mathcal{L}_l , \mathcal{L}_{ace} , denoted as Baseline+ \mathcal{L}_g , Baseline+ \mathcal{L}_l , Baseline+ \mathcal{L}_{ace} , Baseline+ $\mathcal{L}_g+\mathcal{L}_l$, Baseline+ $\mathcal{L}_g+\mathcal{L}_l+\mathcal{L}_{ace}$ (CVRD), respectively. As shown in the table, the Baseline network achieve 83.09%, 71.75%, 5.53, 19.65 in terms of Dice, Jaccard, ASD, and 95HD. With the progressive introduction of \mathcal{L}_g , \mathcal{L}_l , \mathcal{L}_{ace} , our proposed algorithm enjoys consistently improvement gains over the Baseline network, boosting Dice and Jaccard by 5.44%, 7.05%, respectively. Also, the metrics ASD and 95HD are reduced by 2.62 and 10.45, respectively. This further validates the effectiveness of each key component.

4 Conclusion

In this work, we propose CVRD, a semi-supervised contrastive representation distillation framework by leveraging global and local cues to learn voxel-wise representations for volumetric medical image segmentation. Specifically, we propose to use global contrastive and local distillation learning to exploit complex relations among training voxels. To further constrain the segmentation process, we use ACE loss to capture more geometrical information. Experimental results demonstrate that our model yields state-of-the-art performance with generating more accurate boundaries with very limited annotations.

References

1. Bai, W., Chen, C., Tarroni, G., Duan, J., Guitton, F., Petersen, S.E., Guo, Y., Matthews, P.M., Rueckert, D.: Self-supervised learning for cardiac mr image segmentation by anatomical position prediction. In: MICCAI. pp. 541–549. Springer (2019)
2. Bortsova, G., Dubost, F., Hogeweg, L., Katramados, I., de Bruijne, M.: Semi-supervised medical image segmentation via learning consistency under transformations. In: MICCAI. pp. 810–818. Springer (2019)
3. Chaitanya, K., Erdil, E., Karani, N., Konukoglu, E.: Contrastive learning of global and local features for medical image segmentation with limited annotations. arXiv preprint arXiv:2006.10511 (2020)
4. Chen, N., Liu, F., You, C., Zhou, P., Zou, Y.: Adaptive bi-directional attention: Exploring multi-granularity representations for machine reading comprehension. In: ICASSP (2020)
5. Chen, N., You, C., Zou, Y.: Self-supervised dialogue learning for spoken conversational question answering. In: INTERSPEECH (2021)
6. Chen, T., Kornblith, S., Norouzi, M., Hinton, G.: A simple framework for contrastive learning of visual representations. In: ICML. pp. 1597–1607. PMLR (2020)
7. Chen, X., Luo, X., Zhao, Y., Zhang, S., Wang, G., Zheng, Y.: Learning euler’s elastica model for medical image segmentation. arXiv preprint arXiv:2011.00526 (2020)
8. Chen, X., Williams, B.M., Vallabhaneni, S.R., Czanner, G., Williams, R., Zheng, Y.: Learning active contour models for medical image segmentation. In: CVPR. pp. 11632–11640 (2019)
9. Cheng, L., You, C.: Hybrid non-linear dimensionality reduction method framework based on random projections. In: 2016 IEEE International Conference on Cloud Computing and Big Data Analysis (ICCCBDA). pp. 43–48. IEEE (2016)
10. Cheng, L., You, C., Chen, L.: Identification of power line outages based on pmu measurements and sparse overcomplete representation. In: 2016 IEEE 17th International Conference on Information Reuse and Integration (IRI). pp. 343–349. IEEE (2016)
11. Cheng, L., You, C., Guan, Y.: Random projections for non-linear dimensionality reduction. International Journal of Machine Learning and Computing **6**(4), 220–225 (2016)
12. Cheng, L., You, C., Guan, Y., Yu, Y.: Body activity recognition using wearable sensors. In: 2017 Computing Conference. pp. 756–765. IEEE (2017)

13. Doersch, C., Gupta, A., Efros, A.A.: Unsupervised visual representation learning by context prediction. In: ICCV. pp. 1422–1430 (2015)
14. Guha, I., Nadeem, S.A., You, C., Zhang, X., Levy, S.M., Wang, G., Torner, J.C., Saha, P.K.: Deep learning based high-resolution reconstruction of trabecular bone microstructures from low-resolution ct scans using gan-circle. In: Medical Imaging 2020: Biomedical Applications in Molecular, Structural, and Functional Imaging (2020)
15. Hadsell, R., Chopra, S., LeCun, Y.: Dimensionality reduction by learning an invariant mapping. In: CVPR. vol. 2, pp. 1735–1742. IEEE (2006)
16. Hang, W., Feng, W., Liang, S., Yu, L., Wang, Q., Choi, K.S., Qin, J.: Local and global structure-aware entropy regularized mean teacher model for 3d left atrium segmentation. In: MICCAI. pp. 562–571. Springer (2020)
17. Hatamizadeh, A., Sengupta, D., Terzopoulos, D.: End-to-end trainable deep active contour models for automated image segmentation: Delineating buildings in aerial imagery. In: ECCV. pp. 730–746. Springer (2020)
18. He, Y., Yang, G., Chen, Y., Kong, Y., Wu, J., Tang, L., Zhu, X., Dillenseger, J.L., Shao, P., Zhang, S., et al.: Dpa-densebiasnet: Semi-supervised 3d fine renal artery segmentation with dense biased network and deep priori anatomy. In: MICCAI. pp. 139–147. Springer (2019)
19. Hjelm, R.D., Fedorov, A., Lavoie-Marchildon, S., Grewal, K., Bachman, P., Trischler, A., Bengio, Y.: Learning deep representations by mutual information estimation and maximization. In: ICLR (2019)
20. Kass, M., Witkin, A., Terzopoulos, D.: Snakes: Active contour models. International journal of computer vision **1**(4), 321–331 (1988)
21. Laine, S., Aila, T.: Temporal ensembling for semi-supervised learning. arXiv preprint arXiv:1610.02242 (2016)
22. Li, G., Luo, S., You, C., Getzin, M., Zheng, L., Wang, G., Gu, N.: A novel calibration method incorporating nonlinear optimization and ball-bearing markers for cone-beam ct with a parameterized trajectory. Medical physics **46**(1), 152–164 (2019)
23. Li, S., Zhang, C., He, X.: Shape-aware semi-supervised 3d semantic segmentation for medical images. In: MICCAI. pp. 552–561. Springer (2020)
24. Li, X., Yu, L., Chen, H., Fu, C.W., Heng, P.A.: Semi-supervised skin lesion segmentation via transformation consistent self-ensembling model. arXiv preprint arXiv:1808.03887 (2018)
25. Liu, F., Wu, X., You, C., Ge, S., Zou, Y., Sun, X.: Aligning source visual and target language domains for unpaired video captioning. IEEE Transactions on Pattern Analysis and Machine Intelligence (2021)
26. Liu, F., You, C., Wu, X., Ge, S., Sun, X., et al.: Auto-encoding knowledge graph for unsupervised medical report generation. In: NeurIPS (2021)
27. Lyu, Q., You, C., Shan, H., Wang, G.: Super-resolution mri through deep learning. arXiv preprint arXiv:1810.06776 (2018)
28. Ma, H., Chen, T., Hu, T.K., You, C., Xie, X., Wang, Z.: Good students play big lottery better. arXiv preprint arXiv:2101.03255 **3** (2021)
29. Ma, J., He, J., Yang, X.: Learning geodesic active contours for embedding object global information in segmentation cnns. IEEE Transactions on Medical Imaging (2020)
30. Milletari, F., Navab, N., Ahmadi, S.A.: V-net: Fully convolutional neural networks for volumetric medical image segmentation. In: 3DV. pp. 565–571. IEEE (2016)
31. Misra, I., Maaten, L.v.d.: Self-supervised learning of pretext-invariant representations. In: CVPR. pp. 6707–6717 (2020)

32. Nie, D., Gao, Y., Wang, L., Shen, D.: Asdnet: Attention based semi-supervised deep networks for medical image segmentation. In: MICCAI. pp. 370–378. Springer (2018)
33. Noroozi, M., Favaro, P.: Unsupervised learning of visual representations by solving jigsaw puzzles. In: ECCV. pp. 69–84. Springer (2016)
34. Oord, A.v.d., Li, Y., Vinyals, O.: Representation learning with contrastive predictive coding. arXiv preprint arXiv:1807.03748 (2018)
35. Taleb, A., Loetzsch, W., Danz, N., Severin, J., Gaertner, T., Bergner, B., Lippert, C.: 3d self-supervised methods for medical imaging. In: NeurIPS. pp. 18158–18172 (2020)
36. Tarvainen, A., Valpola, H.: Mean teachers are better role models: Weight-averaged consistency targets improve semi-supervised deep learning results. In: NeurIPS. pp. 1195–1204 (2017)
37. Tian, Y., Krishnan, D., Isola, P.: Contrastive multiview coding. arXiv preprint arXiv:1906.05849 (2019)
38. Wang, X., Gupta, A.: Unsupervised learning of visual representations using videos. In: ICCV. pp. 2794–2802 (2015)
39. Wu, Z., Xiong, Y., Stella, X.Y., Lin, D.: Unsupervised feature learning via non-parametric instance discrimination. In: CVPR (2018)
40. Xu, W., Zhou, P., You, C., Zou, Y.: Semantic transportation prototypical network for few-shot intent detection. In: INTERSPEECH (2021)
41. Xue, Y., Tang, H., Qiao, Z., Gong, G., Yin, Y., Qian, Z., Huang, C., Fan, W., Huang, X.: Shape-aware organ segmentation by predicting signed distance maps. In: AAAI (2020)
42. Yang, L., Ghosh, R.P., Franklin, J.M., Chen, S., You, C., Narayan, R.R., Melcher, M.L., Liphardt, J.T.: Nuset: A deep learning tool for reliably separating and analyzing crowded cells. PLoS computational biology (2020)
43. You, C., Chen, N., Liu, F., Yang, D., Zou, Y.: Towards data distillation for end-to-end spoken conversational question answering. arXiv preprint arXiv:2010.08923 (2020)
44. You, C., Chen, N., Zou, Y.: Contextualized attention-based knowledge transfer for spoken conversational question answering. In: INTERSPEECH (2021)
45. You, C., Chen, N., Zou, Y.: Knowledge distillation for improved accuracy in spoken question answering. In: ICASSP (2021)
46. You, C., Chen, N., Zou, Y.: MRD-Net: Multi-Modal Residual Knowledge Distillation for Spoken Question Answering. In: IJCAI (2021)
47. You, C., Chen, N., Zou, Y.: Self-supervised contrastive cross-modality representation learning for spoken question answering. arXiv preprint arXiv:2109.03381 (2021)
48. You, C., Li, G., Zhang, Y., Zhang, X., Shan, H., Li, M., Ju, S., Zhao, Z., Zhang, Z., Cong, W., et al.: CT super-resolution GAN constrained by the identical, residual, and cycle learning ensemble (gan-circle). IEEE Transactions on Medical Imaging **39**(1), 188–203 (2019)
49. You, C., Wang, Q., Sun, C.: sbilsan: Stacked bidirectional self-attention lstm network for anomaly detection and diagnosis from system logs. In: Proceedings of SAI Intelligent Systems Conference. pp. 777–793. Springer (2021)
50. You, C., Yang, J., Chapiro, J., Duncan, J.S.: Unsupervised wasserstein distance guided domain adaptation for 3d multi-domain liver segmentation. In: Interpretable and Annotation-Efficient Learning for Medical Image Computing. pp. 155–163. Springer International Publishing (2020)

51. You, C., Yang, L., Zhang, Y., Wang, G.: Low-Dose CT via Deep CNN with Skip Connection and Network in Network. In: *Developments in X-Ray Tomography XII*. vol. 11113, p. 111131W. International Society for Optics and Photonics (2019)
52. You, C., Yang, Q., Gjesteb, L., Li, G., Ju, S., Zhang, Z., Zhao, Z., Zhang, Y., Cong, W., Wang, G., et al.: Structurally-sensitive multi-scale deep neural network for low-dose CT denoising. *IEEE Access* **6**, 41839–41855 (2018)
53. You, C., Zhou, Y., Zhao, R., Staib, L., Duncan, J.S.: Simcvd: Simple contrastive voxel-wise representation distillation for semi-supervised medical image segmentation. *arXiv preprint arXiv:2108.06227* (2021)
54. Yu, L., Wang, S., Li, X., Fu, C.W., Heng, P.A.: Uncertainty-aware self-ensembling model for semi-supervised 3d left atrium segmentation. In: *MICCAI*. pp. 605–613. Springer (2019)
55. Zhang, M., Dong, B., Li, Q.: Deep active contour network for medical image segmentation. In: *MICCAI*. pp. 321–331. Springer (2020)
56. Zhang, Y., Yang, L., Chen, J., Fredericksen, M., Hughes, D.P., Chen, D.Z.: Deep adversarial networks for biomedical image segmentation utilizing unannotated images. In: *MICCAI*. pp. 408–416. Springer (2017)
57. Zheng, H., Lin, L., Hu, H., Zhang, Q., Chen, Q., Iwamoto, Y., Han, X., Chen, Y.W., Tong, R., Wu, J.: Semi-supervised segmentation of liver using adversarial learning with deep atlas prior. In: *MICCAI*. pp. 148–156. Springer (2019)
58. Zhuang, X., Li, Y., Hu, Y., Ma, K., Yang, Y., Zheng, Y.: Self-supervised feature learning for 3d medical images by playing a rubik’s cube. In: *MICCAI*. pp. 420–428. Springer (2019)